DMD Fast Forward. Published on June 4, 2007 as doi:10.1124/dmd.107.015636

DMD #15636

Data-based Mathematical Modeling of Vectorial Transport Across Double-transfected Polarized Cells*

Kilian Bartholomé, Maria Rius, Katrin Letschert, Daniela Keller, Jens Timmer, and Dietrich Keppler

Institute for Physics, University of Freiburg, Hermann-Herder-Str. 3, 79104 Freiburg, Germany (K.B., J.T.) and Division of Tumor Biochemistry, German Cancer Research Center, Im Neuenheimer Feld 280, 69120 Heidelberg, Germany (M.R., K.L., D.K., D.K.)

DMD Fast Forward. Published on June 4, 2007 as DOI: 10.1124/dmd.107.015636
This article has not been copyedited and formatted. The final version may differ from this version.

Running Title: Mathematical Modeling of Vectorial Transport

Corresponding author:

Dr. Dietrich Keppler

Division of Tumor Biochemistry, German Cancer Research Center,

Im Neuenheimer Feld 280,

69120 Heidelberg, Germany

Tel: +49-6221-422400

Fax: +49-6221-422402

E-mail: d.keppler@dkfz.de

Total number of text pages: 27 pages

Number of tables: 1

Number of figures: 7

Number of references: 26

Number of words in the abstract: 250 words

Number of words in the introduction: 336 words

Number of words in the discussion: 813 words

Supplemental data including 3 figures and 2 tables are provided in a separate file

Nonstandard Abbreviations: ABCC2, human ATP-binding cassette transporter, subfamily C, member 2; Abcc4, canine ATP-binding cassette transporter, subfamily C, member 4; BSP, bromosulfophthalein; $Endo_{ex\text{-}ap}$, apical endogenous efflux transporter; $Endo_{ex\text{-}bl}$, basolateral endogenous efflux transporter; $Endo_{in\text{-}bl}$, basolateral

endogenous uptake transporter; MDCKII, Madin-Darby canine kidney cells strain II; OATP1B3, human organic anion-transporting polypeptide, member 1B3.

DMD Fast Forward. Published on June 4, 2007 as DOI: 10.1124/dmd.107.015636
This article has not been copyedited and formatted. The final version may differ from this version.

Abstract

Vectorial transport of endogenous small molecules, toxins, and drugs across polarized epithelial cells contributes to their half-life in the organism and to detoxification. To study vectorial transport in a quantitative manner, an in vitro model was used that includes polarized MDCKII cells stably expressing the recombinant human uptake transporter OATP1B3 in their basolateral membrane and the recombinant ATP-driven efflux pump ABCC2 in their apical membrane. These double-transfected cells enabled mathematical modeling of the vectorial transport of the anionic prototype substance bromosulfophthalein (BSP) that has frequently been used to examine hepatobiliary transport. Time-dependent analyses of ^{3}H-labeled BSP in the basolateral, intracellular, and apical compartments of cells cultured on filter membranes and efflux experiments in cells preloaded with BSP were performed. A mathematical model was fitted to the experimental data. Data-based modeling was optimized by including endogenous transport processes, in addition to the recombinant transport proteins. The predominant contributions to the overall vectorial transport of BSP were mediated by OATP1B3 (44%) and ABCC2 (28%). Model comparison predicted a previously unrecognized endogenous basolateral efflux process as a negative contribution to total vectorial transport, amounting to 19%, which is in line with the detection of the basolateral efflux pump Abcc4 in MDCKII cells. Rate-determining steps in the vectorial transport were identified by calculating control coefficients. Data-based mathematical modeling of vectorial transport of BSP as a model substance resulted in a quantitative description of this process and its components. The same systems biology approach may be applied to other cellular systems and to different substances.

DMD Fast Forward. Published on June 4, 2007 as DOI: 10.1124/dmd.107.015636
This article has not been copyedited and formatted. The final version may differ from this version.

Introduction

Vectorial transport of small molecules is an important process in polarized cells. Uptake across the basolateral membrane and efflux across the apical membrane domain of polarized cells contribute to the elimination and often detoxification of substances. In mammals, endogenous compounds and drugs are taken up from the blood into hepatocytes and subsequently effluxed mainly into bile.

Several factors affect vectorial transport of small molecules. First, unidirectional transport does not occur at a sufficient rate in the absence of the respective transport proteins in the basolateral and apical membranes, as evidenced by studies in hereditary mutants lacking certain transport proteins (Jansen et al., 2001; Keppler et al., 2001; Schinkel and Jonker, 2003) or in cell lines stably transfected with cDNAs encoding transport proteins (Cui et al., 2001; Sasaki et al., 2002; Hagenbuch and Meier, 2004). Second, it is affected in the intact organism by blood flow, intravascular binding to proteins, and intracellular metabolism.

To build a mathematical model of vectorial transport, we used a well-defined cellular system developed earlier (Cui et al., 2001). Polarized cells grown on filter membrane supports were stably transfected with cDNAs encoding the human uptake transporter for organic anions, OATP1B3 (König et al., 2000), and the human apical conjugate export pump ABCC2, also known as multidrug resistance protein 2 (MRP2) (Büchler et al., 1996). Such double-transfected cells exhibit transporter-mediated substrate flux from the basolateral to the apical compartment and, for most compounds, very little intracellular metabolism (Cui et al., 2001; Keppler, 2005; Letschert et al., 2005). Bromosulfophthalein (BSP) is a substrate for both transport proteins, OATP1B3 (König et al., 2000) and ABCC2 (Cui et al., 2001). Moreover, BSP is an established test compound for studies of hepatobiliary elimination in humans and animals (Wolkoff, 1994). Mathematical modeling was performed in this

DMD Fast Forward. Published on June 4, 2007 as DOI: 10.1124/dmd.107.015636
This article has not been copyedited and formatted. The final version may differ from this version.

focused cellular system mediating the vectorial transport of BSP. The same modeling approach can be applied to other polarized cellular systems and to a variety of different substances, thus opening the perspective of quantitative and predictive modeling and understanding of vectorial transport systems.

DMD Fast Forward. Published on June 4, 2007 as DOI: 10.1124/dmd.107.015636
This article has not been copyedited and formatted. The final version may differ from this version.

Methods

Cell Culture and Cell Lines. Madin-Darby canine kidney cells strain II (MDCKII) permanently expressing high levels of recombinant human OATP1B3 or OATP1B3 together with ABCC2 were cultured as described (Cui et al., 2001; see Fig. 1).

Immunofluorescence Microscopy. MDCKII cells were grown on ThinCert membrane inserts (diameter 6 mm; pore size 0.4 µm; pore density 1 x 10^8/cm^2; Greiner Bio-One, Frickenhausen, Germany; Letschert et al., 2005) for 3 days at confluence and induced with 10 mM sodium butyrate for 24 h to enhance the expression of recombinant proteins (Cui et al., 1999). Fixation and permeabilization were performed as described (Cui et al., 2001). OATP1B3 was detected by the antiserum SKT (König et al., 2000), ABCC2 was detected by the antiserum EAG (Cui et al., 1999), and canine Abcc4 was detected by the purified antiserum SNG (Rius et al., 2003). Nuclei were stained with propidium iodide. Confocal laser scanning microscopy was performed with a LSM 510 Meta apparatus from Carl Zeiss (Jena, Germany).

Transport Studies. [^{3}H]Bromosulfophthalein (BSP, 0.5 TBq/mmol) was obtained from Hartmann Analytic (Braunschweig, Germany) (Cui et al., 2001). MDCKII cells were grown on ThinCert membrane inserts (diameter, 24 mm; pore size, 0.4 µm; pore density, 1 x 10^8/cm^2; Greiner Bio-One, Frickenhausen, Germany) for 3 days at confluence and induced with 10 mM sodium butyrate for 24 h (Cui et al., 1999). The cells were washed in prewarmed (37°C) transport buffer (142 mM NaCl, 5 mM KCl, 1 mM KH_2PO_4, 1.2 mM $MgSO_4$, 1.5 mM $CaCl_2$, 5 mM glucose, and 12.5 mM HEPES, pH 7.3). The ^{3}H-labeled substrate was dissolved in transport buffer and added to the basolateral compartment (1.5 ml) at the concentration indicated. After incubation at

DMD Fast Forward. Published on June 4, 2007 as DOI: 10.1124/dmd.107.015636
This article has not been copyedited and formatted. The final version may differ from this version.

37°C, radioactivity in the apical compartment (1.0 ml) was measured by sampling of aliquots from the apical compartment. Cells were washed twice with ice-cold transport buffer containing 0.5% bovine serum albumin and three times with ice-cold transport buffer. Intracellular radioactivity was determined after lyzing the cells with 0.2% sodium dodecylsulfate.

For preloading studies, cells were washed after incubation at 37°C with the labeled substrate as described above. Subsequently, cells were further incubated at 37°C with transport buffer (1.0 ml in the basolateral and 1.0 ml in the apical compartment) in the absence of labeled substrate and radioactivity was determined as mentioned above.

The paracellular leakage was determined by addition of 1 µM [^{3}H]inulin (Biotrend, Köln, Germany) to the basolateral compartment and measurement of the radioactivity appearing in the apical compartment. The paracellular leakage was less than 2% of the radioactivity added for all MDCKII cell clones examined in this study.

Numerical Analysis. Ordinary differential equations were derived from the model depicted in Fig. 2 by assuming Michaelis-Menten kinetics in the linear regime. The kinetic behavior of the transporters OATP1B3 (König et al., 2000) and ABCC2 (Cui et al., 1999) has been characterized and Michaelis-Menten constants were determined. The equations were integrated by ODESSA (Leis and Kramer, 1988a; Leis and Kramer, 1988b). To insure that we could identify all parameters while performing the multi-experiment fit, we used a penalized likelihood as cost-function for parameter estimation. This likelihood includes prior knowledge of the parameter distribution (see Supplemental data). The resulting cost function was minimized using an optimization routine of the Gauss-Newton type (Hanson and Haskell, 1982; Peifer and Timmer, 2007). Because measurement errors show a linear dependence on the estimated

DMD Fast Forward. Published on June 4, 2007 as DOI: 10.1124/dmd.107.015636
This article has not been copyedited and formatted. The final version may differ from this version.

mean value, we re-estimated the standard deviations by applying a linear error model to minimize the fluctuations in the estimated standard deviations (see Supplemental data).

DMD Fast Forward. Published on June 4, 2007 as DOI: 10.1124/dmd.107.015636
This article has not been copyedited and formatted. The final version may differ from this version.

Results

The Cell System. MDCKII cells were grown in a polarized fashion on filter membrane supports and transport of BSP, a substrate for both OATP1B3 and ABCC2, was studied in this system. The expression and sorting of the transport proteins were confirmed by immunofluorescence and confocal laser scanning microscopy (Fig. 1). The cell line represents an improved version of the double-transfectant described earlier (Cui et al., 2001).

MDCKII cells were also analyzed for the expression and localization of endogenous transport proteins, as suggested by the mathematical modeling. Endogenous canine Abcc4 was localized to the basolateral membrane of the MDCKII cells (Fig. 1E). Thus, this endogenous basolateral efflux pump functions in addition to the recombinant human transport proteins. ABCC4 has a broad substrate specificity (Kruh et al., 2007) that includes BSP (data not shown). The influxes, effluxes, and concentration pools are summarized in Fig. 2.

Uptake and Efflux Transport in Polarized Cells. To acquire data, several sets of transport experiments were performed. Vectorial transport of labeled BSP was measured over 60 min at high (10 µM, Fig. 3) and low (10 nM, Fig. 4) concentrations. The intracellular content of labeled BSP was significantly higher in MDCKII cells expressing recombinant OATP1B3 than in the control MDCKII cells (Figs. 3-4, lower panels), indicating that OATP1B3 is responsible for the uptake and intracellular accumulation of BSP. The release of BSP into the apical chamber was mainly detected in cells expressing recombinant OATP1B3 together with ABCC2 (upper panels of Figs. 3-4), indicating that ABCC2 in the apical membrane efficiently mediates the efflux of BSP.

DMD Fast Forward. Published on June 4, 2007 as DOI: 10.1124/dmd.107.015636
This article has not been copyedited and formatted. The final version may differ from this version.

To assess the contributions of endogenous transport processes, the cells were preloaded (Fig. 5) by adding [^{3}H]labeled BSP to the basolateral chamber for 30 min. After this preloading time, the amounts of radioactivity effluxed into the apical chamber and into the basolateral chamber (basolateral amount), as well as radioactivity accumulated inside the cells, were determined. BSP was strongly accumulated in cells expressing OATP1B3 and, to a lesser extent, in cells expressing OATP1B3 together with ABCC2 (middle panel of Fig. 5). The MDCKII cells expressing recombinant OATP1B3 and ABCC2 showed the highest efflux of BSP into the apical chamber (upper panel of Fig. 5). However, the major BSP efflux into the basolateral chamber was observed in the cells which had reached the highest intracellular content (lower panel of Fig. 5). This efflux is most probably mediated by the endogenous (canine) Abcc4 of the MDCKII cells (Fig. 1E).

The Mathematical Model. Our model incorporated the effects of several transport factors. First, as can be seen from measurements in MDCKII control cells (Figs. 3-4), there was a small but significant increase of BSP in the intracellular compartment and in the apical chamber. This observation suggests the existence of an endogenous basolateral uptake transporter ($Endo_{in\text{-}bl}$ in Fig. 2) as well as an apical endogenous efflux pump ($Endo_{ex\text{-}ap}$ in Fig. 2). Second, preloading experiments (Fig. 5) indicated the existence of a basolateral efflux pump ($Endo_{ex\text{-}bl}$ in Fig. 2). Third, based on [^{3}H]inulin transport experiments, we observed a low rate (less than 1 % of total transport) of paracellular leakage (data not shown), which was also included in our model. Fourth, to determine the amount of [^{3}H]BSP that bound to cytosolic proteins, we separated the cytosolic protein fraction by centrifugation at 20000 x g and measured the amount of radioactivity in the resulting supernatant. We found that about 86% of the BSP bound to intracellular macromolecules. To account for this

DMD Fast Forward. Published on June 4, 2007 as DOI: 10.1124/dmd.107.015636
This article has not been copyedited and formatted. The final version may differ from this version.

binding, we added intracellular binding sites to the model (x_4 in Fig. 2). Fifth, control experiments without any cultured cells showed a significant amount of BSP bound non-specifically to the filter membrane support. This binding was also included in the model (x_2 in Fig. 2). Finally, the intracellular content of BSP is about 7-times greater for the cells expressing recombinant OATP1B3 than for the control cells when determined at 60 min (Fig. 3). If transcellular diffusion played a significant role, the apical amount of BSP should be much greater for the OATP1B3-expressing cells than for the control cells. Thus, transcellular diffusion seems to be negligible and therefore was not factored into the model.

Assuming Michaelis-Menten kinetics in the linear regime, we derived the ordinary differential equations (Table 1) from the model shown in Fig. 2. This procedure is in accord with similar modeling approaches (Liu and Pang, 2006; Turncliff et al., 2006). The rates of BSP uptake into cells may vary somewhat between different sets of experiments depending on the expression level of OATP1B3. Accordingly, we fitted our model to the data from all of the experiments of the present study by maximizing a penalized likelihood (Good and Gaskins, 1971) as explained in the Supplemental data. The penalized likelihood was introduced to insure that we could identify all parameters for the multi-experiment fit (see Supplemental data). Results of the fits are shown in Figs. 3-5.

We found it necessary to include the endogenous transporters in the model. We compared the complete model (Fig. 2) to models lacking selected endogenous transport processes. Each of the smaller models yielded a significantly worse fit of the data than the complete model (see Supplemental data).

Rate-Determining Steps in Vectorial Transport. Based on our model (Fig. 2), we calculated the contribution of each transport process to the total amount of BSP

DMD Fast Forward. Published on June 4, 2007 as DOI: 10.1124/dmd.107.015636
This article has not been copyedited and formatted. The final version may differ from this version.

transported into the apical chamber. The largest amount of BSP was transported by the recombinant uptake transporter OATP1B3, followed by the recombinant apical efflux pump ABCC2, by the endogenous efflux pump $Endo_{ex\text{-}bl}$ (probably Abcc4), and by the endogenous uptake transporter $Endo_{in\text{-}bl}$ (Fig. 6A). The endogenous apical efflux $Endo_{ex\text{-}ap}$ and paracellular transport contributed the smallest fractions to the total transported amount. OATP1B3 accounted for about 44% of the overall transport, followed by ABCC2 with 28%, and the endogenous efflux pump $Endo_{ex\text{-}bl}$ with about 19% (Fig. 6B). The endogenous transporters $Endo_{in\text{-}bl}$ and $Endo_{ex\text{-}ap}$, and paracellular BSP transport together account for less than 10% of the total transport. Since the endogenous efflux pump $Endo_{ex\text{-}bl}$ (probably Abcc4) transports BSP back into the basolateral chamber, its contribution to the total amount of BSP transported into the apical chamber is actually negative.

Control coefficients have frequently been used in metabolic control analysis to quantify the contribution of a given enzyme to the steady-state flux of metabolites (Conradie et al., 2006; Schuster and Heinrich, 1992). In this analysis, the fractional change of the steady-state flux of a metabolite J is related to the fractional change of an enzyme activity v, defined as $C^J_v = v/J \, dJ/dv$. For our system, we calculated the relationship of the fractional change of the total flux into the apical chamber, $J = dx_5/dt$, to the fractional change of each transport process in our model (Fig. 7). Since the rate for each transport process in our model is linear and has the form $v_j = p_j x_k$, the normalized control coefficients read:

$$C^J_{v_j} = \frac{p_j}{J}\frac{\partial J}{\partial p_j}$$

where p_j is the parameter controlling transport process j. The resulting control coefficients for the double-transfected and MDCKII control cells are depicted in Fig. 7.

DMD Fast Forward. Published on June 4, 2007 as DOI: 10.1124/dmd.107.015636
This article has not been copyedited and formatted. The final version may differ from this version.

For the double-transfected cells, the control coefficients of OATP1B3 and ABCC2 were the dominant transport processes and were rate-determining in our system. This agrees with the fact that each of the single-transfected cells (i.e., OATB1B3 cells or ABCC2 cells; Cui et al., 2001) exhibit significantly less total vectorial transport than the double-transfected cells. For control cells, on the other hand, the control coefficient of the endogenous transporters $Endo_{in\text{-}bl}$ and $Endo_{ex\text{-}ap}$, as well as the paracellular flow, are the main processes. The comparison of the control coefficients of the parental cells with the control coefficients of the double-transfected cells shows that the rate-determining step in vectorial transport clearly depends on the expression level of the respective transport proteins.

DMD Fast Forward. Published on June 4, 2007 as DOI: 10.1124/dmd.107.015636
This article has not been copyedited and formatted. The final version may differ from this version.

Discussion

Vectorial transport across polarized cells controls the half-life of many endogenous and xenobiotic substances in the mammalian organism and contributes to their detoxification and terminal elimination. We developed a mathematical model that describes the best fit to the experimental data from determinations of radioactively labeled BSP in the basolateral compartment, inside the cells, and in the apical compartment. The parameters of the mathematical model described here for the vectorial transport of BSP in double-transfected polarized cells were determined by maximizing a penalized likelihood (Good and Gaskins, 1971) as explained in detail in the Supplemental data. This approach provides new qualitative as well as quantitative insights into the components and the dynamic behavior of vectorial transport. In particular, the role of endogenous transport processes was recognized and quantified, in addition to the role of the transfected recombinant transporters OATP1B3 and ABCC2.

In this study, our data-based mathematical modeling was supported by application of an in vitro cell-culture system that allowed quantitative analyses of a labeled model substance in different compartments at various time points. In several aspects, this biological system with double-transfected polarized cells (Fig. 1) resembles human hepatocytes and the vectorial transport of many substances, including BSP, from the blood circulation into bile (Keppler, 2005).

The model shows excellent agreement with the experimental data. The optimal fit of the model was achieved by maximizing a penalized likelihood (Good and Gaskins, 1971) and required the inclusion of endogenous transport processes of the MDCKII cell, in addition to the stably-expressed recombinant human transporters OATP1B3 and ABCC2. The role of endogenous transport proteins in the MDCKII cells was addressed by preloading experiments, which enabled quantitative measurements of

efflux from the cells into the apical and into the basolateral chamber. The excellent agreement of the model with the experimental data indicates that transcellular diffusion was not required as an additional parameter, at least in the case of the hydrophilic BSP. A similar modeling approach could be taken with the introduction of other recombinant transport proteins, such as uptake mediated by OATP2B1 and the efflux pump ABCC2 (Kopplow et al., 2005) or the sodium-dependent bile acid uptake transporter NTCP and the efflux pump ABCB11 (Mita et al., 2006).

As expected, the greatest contributions to the transport of BSP came from recombinant OATP1B3 and ABCC2 (44% and 28% of total transport, respectively). Surprisingly, endogenous basolateral efflux, designated $Endo_{ex\text{-}bl}$, amounted to 19%, which is in line with the significant amount of the endogenous protein Abcc4 in the basolateral membrane. In hepatocytes, basolateral efflux pumps, including ABCC3 and ABCC4, also play an important role in overall transport of small molecules (Rius et al., 2003).The basolateral efflux in the MDCKII cells was initially indicated by model comparison, leading to the best fit with the experimental data. This efflux was verified and further quantified by preloading experiments. Notably, all other processes integrated into our model together amount to less than 10% of the transport. This small contribution is in accord with the normalized control coefficients for the fluxes in the double-transfected cells. Thus, variations in the activity of OATP1B3 or ABCC2 have the greatest effect on total flux. Since the control coefficients for OATP1B3 and ABCC2 are similar, a rate-determining step cannot be singled out in this cellular system. This will be different when the activity of one of the six processes described in our model is significantly changed, as can be seen for the control coefficients of the MDCKII control cells where other partial processes dominate total vectorial flux.

DMD Fast Forward. Published on June 4, 2007 as DOI: 10.1124/dmd.107.015636
This article has not been copyedited and formatted. The final version may differ from this version.

In conclusion, the polarized cell system for studies on vectorial transport (Cui et al., 2001; Sasaki et al., 2002) was successfully used for data-based mathematical modeling and resulted in the quantification of individual transport steps in a complex system. This quantitative modeling greatly expands the mostly qualitative previous knowledge on the vectorial transport of endogenous and xenobiotic substances. Accordingly, predictions can be made for the time-course of transport and for the relative contribution of single transport steps to the overall transport. Calculation of control coefficients enabled the identification of rate-determining single steps in overall vectorial transport. Moreover, the modeling approach in this study has been useful for the identification of previously unexpected partial processes, such as the quantitatively important basolateral efflux ($Endo_{ex\text{-}bl}$). This additional transport process is well explained by the detection of endogenous Abcc4 in the MDCKII cells. Inclusion of this process was necessary to obtain excellent agreement between the experimental data and the mathematical model. Thus, data-based quantitative mathematical modeling led to new qualitative as well as quantitative insight into the biological system. In this study, we focused on BSP as a well-known model substance for the analysis of hepatobiliary elimination. However, this modeling approach may be applied to other substances, e.g. cholecystokinin octapeptide CCK-8, the vectorial transport of which has been characterized recently (Letschert et al., 2005), and other polarized cellular systems, such as quadruple-transfected MDCKII cells (Kopplow, 2005)

Acknowledgments

We thank Yunhai Cui and Jörg König for their assistance in the initial phase of our studies, Anne Nies and Manuela Brom for their help in generating the figures, and Gary Howard for editorial assistance.

DMD Fast Forward. Published on June 4, 2007 as DOI: 10.1124/dmd.107.015636
This article has not been copyedited and formatted. The final version may differ from this version.

References

Büchler M, König J, Brom M, Kartenbeck J, Spring H, Horie T and Keppler D (1996) cDNA cloning of the hepatocyte canalicular isoform of the multidrug resistance protein, cMRP, reveals a novel conjugate export pump deficient in hyperbilirubinemic mutant rats. *J Biol Chem* **271**:15091-15098.

Conradie R, Westerhoff HV, Rohwer JM, Hofmeyr JH and Snoep JL (2006) Summation theorems for flux and concentration control coefficients of dynamic systems. *Syst Biol (Stevenage)* **153**:314-317.

Cui Y, König J, Buchholz U, Spring H, Leier I and Keppler D (1999) Drug resistance and ATP-dependent conjugate transport mediated by the apical multidrug resistance protein, MRP2, permanently expressed in human and canine cells. *Mol Pharmacol* **55**:929-937.

Cui Y, König J and Keppler D (2001) Vectorial transport by double-transfected cells expressing the human uptake transporter SLC21A8 and the apical export pump ABCC2. *Mol Pharmacol* **60**:934-943.

Good IJ and Gaskins RA (1971) Non-parametric roughness penalties for probability densities. *Biometrika* **58**:255-277.

Hagenbuch B and Meier PJ (2004) Organic anion transporting polypeptides of the OATP/ SLC21 family: phylogenetic classification as OATP/ SLCO superfamily, new nomenclature and molecular/functional properties. *Pflügers Arch* **447**:653-665.

Hanson RJ and Haskell KH (1982) Algorithm 587: two algorithms for the linearly constrained least squares problem. *ACM Trans Math Softw* **8**:323-333.

Jansen PL, Müller M and Sturm E (2001) Genes and cholestasis. *Hepatology* **34**:1067-1074.

Keppler D (2005) Uptake and efflux transporters for conjugates in human hepatocytes. *Methods Enzymol* **400**:531-542.

Keppler D, König J and Nies AT (2001) Conjugate export pumps of the multidrug resistance protein (MRP) family in liver, in *The Liver: Biology and Pathobiology* (Arias IM, Boyer JL, Chisari FV, Fausto N, Schachter D and Shafritz DA eds) pp 373-382, Lippincott Williams & Wilkins, New York.

König J, Cui Y, Nies AT and Keppler D (2000) Localization and genomic organization of a new hepatocellular organic anion transporting polypeptide. *J Biol Chem* **275**:23161-23168.

Kopplow K, Letschert K, König J, Walter B and Keppler D (2005) Human hepatobiliary transport of organic anions analyzed by quadruple-transfected cells. *Mol Pharmacol* **68**:1031-1038.

Kruh GD, Belinsky MG, Gallo JM and Lee K (2007) Physiological and pharmacological functions of Mrp2, Mrp3 and Mrp4 as determined from recent studies on gene-disrupted mice. *Cancer Metastasis Rev* **in press**.

Leis JR and Kramer MA (1988a) ODESSA - an ordinary differential equation solver with explicit simultaneous sensitivity analysis. *ACM Trans Math Softw* **14**:61-67.

Leis JR and Kramer MA (1988b) The simultaneous solution and sensitivity analysis of systems described by ordinary differential equations". *ACM Trans Math Softw* **14**:45-60.

Letschert K, Komatsu M, Hummel-Eisenbeiss J and Keppler D (2005) Vectorial transport of the peptide CCK-8 by double-transfected MDCKII cells stably expressing the organic anion transporter OATP1B3 (OATP8) and the export pump ABCC2. *J Pharmacol Exp Ther* **313**:549-556.

Liu L and Pang KS (2006) An integrated approach to model hepatic drug clearance. *Eur J Pharm Sci* **29**:215-230.

Mita S, Suzuki H, Akita H, Hayashi H, Onuki R, Hofmann AF and Sugiyama Y (2006) Vectorial transport of unconjugated and conjugated bile salts by monolayers of LLC-PK1 cells doubly transfected with human NTCP and BSEP or with rat Ntcp and Bsep. *Am J Physiol Gastrointest Liver Physiol* **290**:G550-G556.

Peifer M and Timmer J (2007) Parameter estimation in ordinary differential equations for biochemical processes using the method of multiple shooting. *IET Syst Biol* **in press**.

Rius M, Nies AT, Hummel-Eisenbeiss J, Jedlitschky G and Keppler D (2003) Cotransport of reduced glutathione with bile salts by MRP4 (ABCC4) localized to the basolateral hepatocyte membrane. *Hepatology* **38**:374-384.

Sasaki M, Suzuki H, Ito K, Abe T and Sugiyama Y (2002) Transcellular transport of organic anions across a double-transfected Madin-Darby canine kidney II cell monolayer expressing both human organic anion-transporting polypeptide (OATP2/SLC21A6) and Multidrug resistance-associated protein 2 (MRP2/ABCC2). *J Biol Chem* **277**:6497-6503.

Schinkel AH and Jonker JW (2003) Mammalian drug efflux transporters of the ATP binding cassette (ABC) family: an overview. *Adv Drug Deliv Rev* **55**:3-29.

Schuster S and Heinrich R (1992) The definitions of metabolic control analysis revisited. *Biosystems* **27**:1-15.

Turncliff RZ, Hoffmaster KA, Kalvass JC, Pollack GM and Brouwer KL (2006) Hepatobiliary disposition of a drug/metabolite pair: Comprehensive pharmacokinetic modeling in sandwich-cultured rat hepatocytes. *J Pharmacol Exp Ther* **318**:881-889.

Westerhoff HV (2007) Mathematical and theoretical biology for systems biology, and then ... vice versa. *J Math Biol* **54**:147-150.

Wolkoff AW (1994) Hepatocyte basolateral membrane organic anion transporters, in *The Liver: Biology and Pathobiology* (Arias IM, Boyer JL, Chisari FV, Fausto N, Schachter D and Shafritz DA eds) pp 179-188, Lippincott Williams & Wilkins, New York.

Footnotes

*****This work was supported by the German Cancer Research Center, by the program on systems biology of the Bundesministerium für Forschung und Technologie (grants to J. T. (0313074A) and D. K. (31P3111), and by the Wilhelm Sander Foundation, München (grant 2004.101.1).

DMD Fast Forward. Published on June 4, 2007 as DOI: 10.1124/dmd.107.015636
This article has not been copyedited and formatted. The final version may differ from this version.

Legends for Figures

Fig. 1. Immunolocalization of recombinant human OATP1B3, ABCC2, and endogenous Abcc4 in canine MDCKII cells. Cells were grown in a polarized fashion on membrane inserts and analyzed by confocal laser scanning microscopy for the localization of OATP1B3 (green in A and B), ABCC2 (red in C and D), and canine Abcc4 (orange in E). Nuclei are stained in blue. A, C and E are en face images at the top of the cell monolayers; B and D are vertical sections through the cell monolayers at positions indicated by the white lines in A and C. Scale bars = 10 µm.

Fig. 2. Cellular basis for the mathematical model of the vectorial transport in polarized MDCKII cells. The cell system comprises three major compartments: the basolateral compartment [x_1], the intracellular compartment [x_3], and the apical compartment [x_5]. The extracellular binding sites [x_2] represent the non-specific binding of the substrate to the filter membrane, and the intracellular binding sites [x_4] represent the binding of the substrate to intracellular proteins. Both extracellular and intracellular binding sites have been experimentally verified. Six different transport processes were identified: the basolateral uptake mediated by human OATP1B3, the apical efflux mediated by human ABCC2, the basolateral endogenous uptake $Endo_{in\text{-}bl}$, and the basolateral and the apical endogenous efflux processes, $Endo_{ex\text{-}bl}$ and $Endo_{ex\text{-}ap}$, respectively, as well as the paracellular leakage.

Fig. 3. Mathematical modeling of the time-dependent transport of bromosulfophthalein (BSP) by the polarized cells. Control cells, cells expressing OATP1B3, or cells expressing OATP1B3 together with ABCC2 were grown as described in “Methods”. Cells were incubated with 10 µM [^{3}H]BSP in the basolateral

DMD Fast Forward. Published on June 4, 2007 as DOI: 10.1124/dmd.107.015636
This article has not been copyedited and formatted. The final version may differ from this version.

chamber. Radioactivity inside the cells (intracellular content, $x_3 + x_4$) and in the apical chamber (apical amount, x_5) was determined at the time points indicated. Data points with error bars represent mean values, given as nmol per mg cellular protein ± S.D., from a triplicate determination reproduced independently at least once. The solid lines result from the mathematical modeling of the measured data.

Fig. 4. Mathematical modeling of the transport of bromosulfophthalein (BSP) in polarized cells. Cell lines described in the legend to Fig. 3 were incubated with [^{3}H]BSP in the basolateral chamber; however, the substrate concentration was only 10 nM. Levels of radioactivity in cells (intracellular content, $x_3 + x_4$) and in the apical chamber (apical amount, x_5) were determined. Data points with error bars represent mean values, given as pmol per mg cellular protein ± S.D., from a triplicate determination reproduced independently at least once. The solid lines were derived from the mathematical modeling of the measured points.

Fig. 5. Mathematical modeling of the time-dependent changes after preloading of cells with [^{3}H]bromosulfophthalein (BSP). Cells described in the legend to Fig. 3 were preloaded with 10 µM [^{3}H]BSP in the basolateral chamber for 30 min. After extensive washing, the amounts of radioactivity in the basolateral chamber (basolateral amount, x_1), inside the cells (intracellular content, $x_3 + x_4$), and in the apical chamber (apical amount, x_5) were determined. Data points with error bars represent mean values, given as nmol per mg cellular protein ± S.D., from a triplicate determination reproduced independently at least once, and solid lines were derived from the mathematical modeling of the data.

Fig. 6. Mathematical simulation of the different transport processes in double-transfected polarized MDCKII cells. (A) Total amount of BSP transported in each of the different transport processes over time. (B) Relative contributions of the different processes during 60 min of BSP transport.

Fig. 7. Control coefficients for the different transport processes. Control coefficients were calculated for different transport processes (Schuster and Heinrich, 1992; Westerhoff, 2007; see Results) in double-transfected cells and control (parental) MDCKII cells. The control coefficients of OATP1B3 and ABCC2 are predominating in the double-transfected cells (colored columns). In control cells (open columns) the endogenous transport processes $Endo_{in\text{-}bl}$, and $Endo_{ex\text{-}ap}$, as well as paracellular flux are the predominating processes.

DMD Fast Forward. Published on June 4, 2007 as DOI: 10.1124/dmd.107.015636
This article has not been copyedited and formatted. The final version may differ from this version.

Tables

Table 1. Ordinary differential equations deduced from the model by assuming linearized Michaelis-Menten kinetics. Here, x_1 is the basolateral amount and x_2 is BSP bound non-specifically to the filter membranes. Unbound intracellular BSP is denoted by x_3, whereas x_4 is BSP bound to intracellular binding proteins and x_5 is the apical amount of BSP. The rate constants p_1 and p_2 for OATP1B3 and ABCC2, as well as p_3, p_4, and p_5 for $Endo_{in\text{-}bl}$, $Endo_{ex\text{-}bl}$, and $Endo_{ex\text{-}ap}$ are proportional to the respective concentrations of the transporters. V_{bl} and V_{ap} denote the volume of the basolateral and the apical chamber, respectively.

$$\frac{dx_1}{dt} = -p_1x_1 - p_3x_1 + p_4x_3 - p_6x_1(p_8 - x_2) + p_7x_2 - p_{12}\left(\frac{x_1}{V_{bl}} - \frac{x_5}{V_{ap}}\right)$$

$$\frac{dx_2}{dt} = p_6x_1(p_8 - x_2) - p_7x_2$$

$$\frac{dx_3}{dt} = p_1x_1 - p_2x_3 + p_3x_1 - p_4x_3 - p_5x_3 - p_9x_3(p_{11} - x_4) + p_{10}x_4$$

$$\frac{dx_4}{dt} = p_9x_3(p_{11} - x_4) - p_{10}x_4$$

$$\frac{dx_5}{dt} = p_2x_3 + p_5x_3 + p_{12}\left(\frac{x_1}{V_{bl}} - \frac{x_5}{V_{ap}}\right)$$

DMD Fast Forward. Published on June 4, 2007 as DOI: 10.1124/dmd.107.015636
This article has not been copyedited and formatted. The final version may differ from this version.

Fig. 1

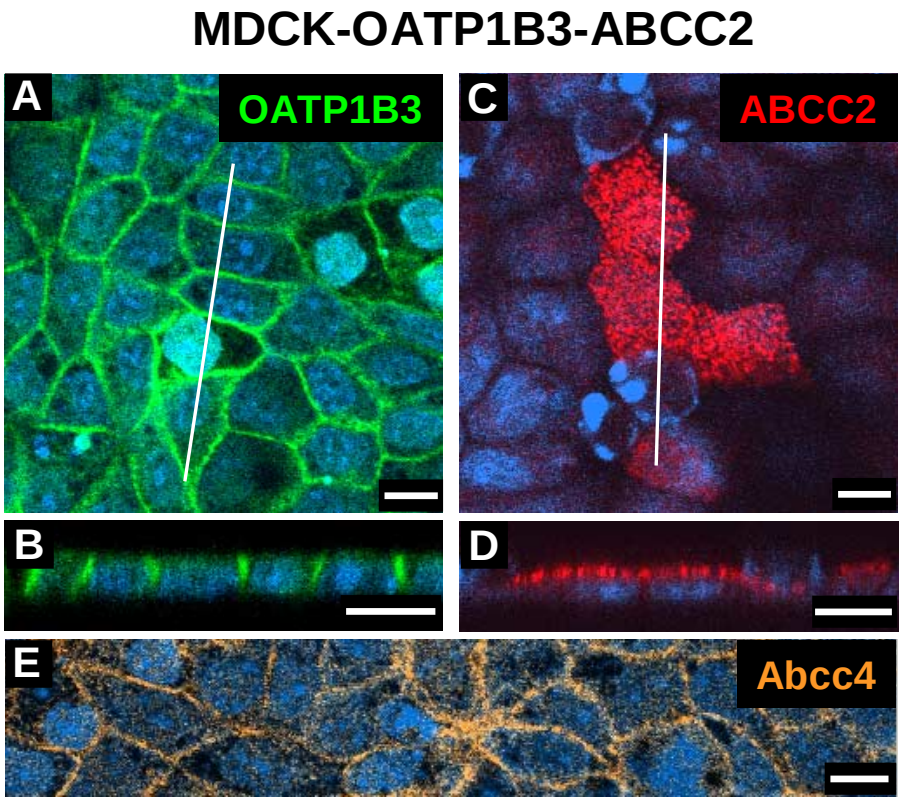

Fig. 2

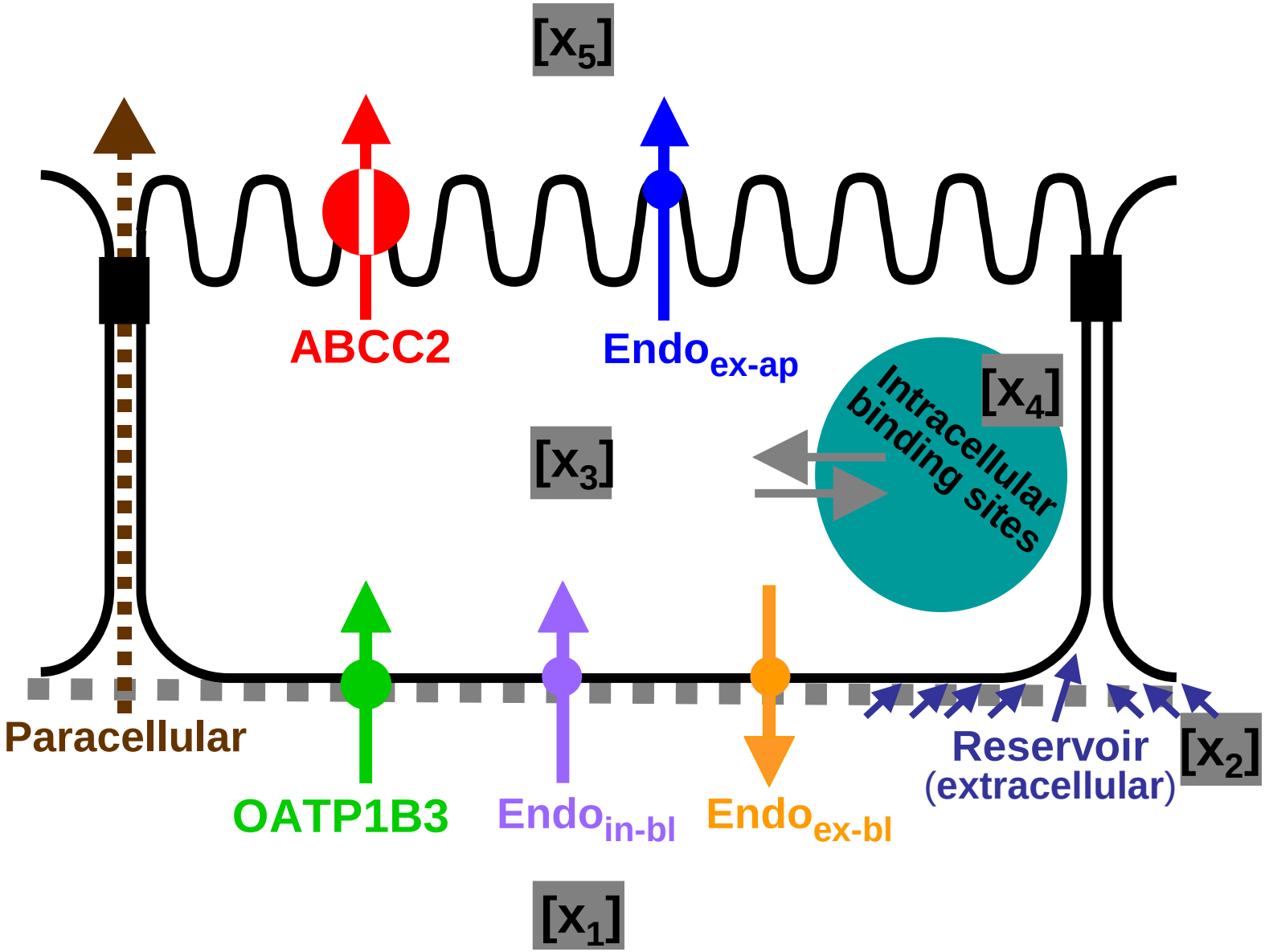

DMD Fast Forward. Published on June 4, 2007 as DOI: 10.1124/dmd.107.015636
This article has not been copyedited and formatted. The final version may differ from this version.

Fig. 3

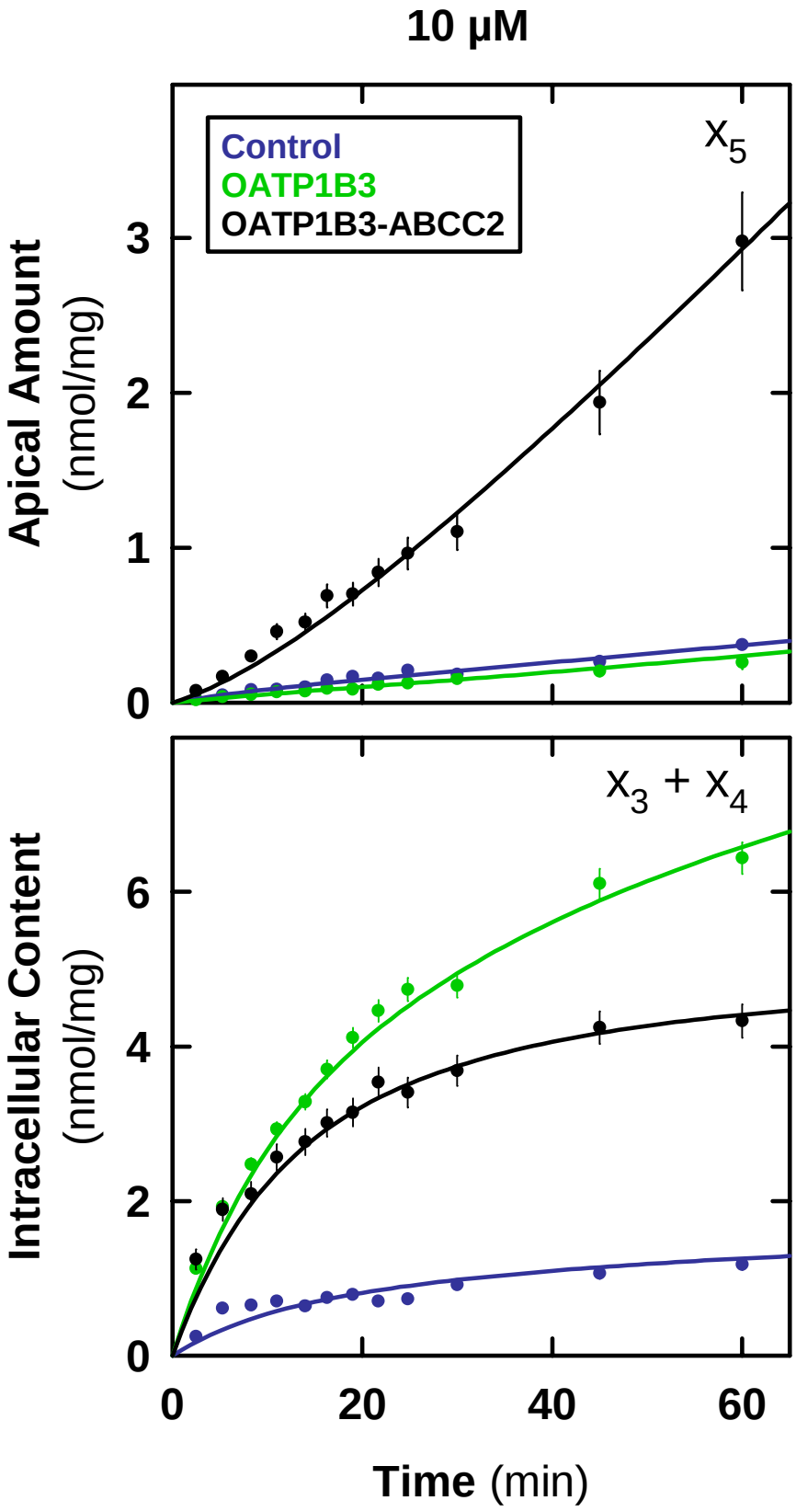

DMD Fast Forward. Published on June 4, 2007 as DOI: 10.1124/dmd.107.015636
This article has not been copyedited and formatted. The final version may differ from this version.

Fig. 4

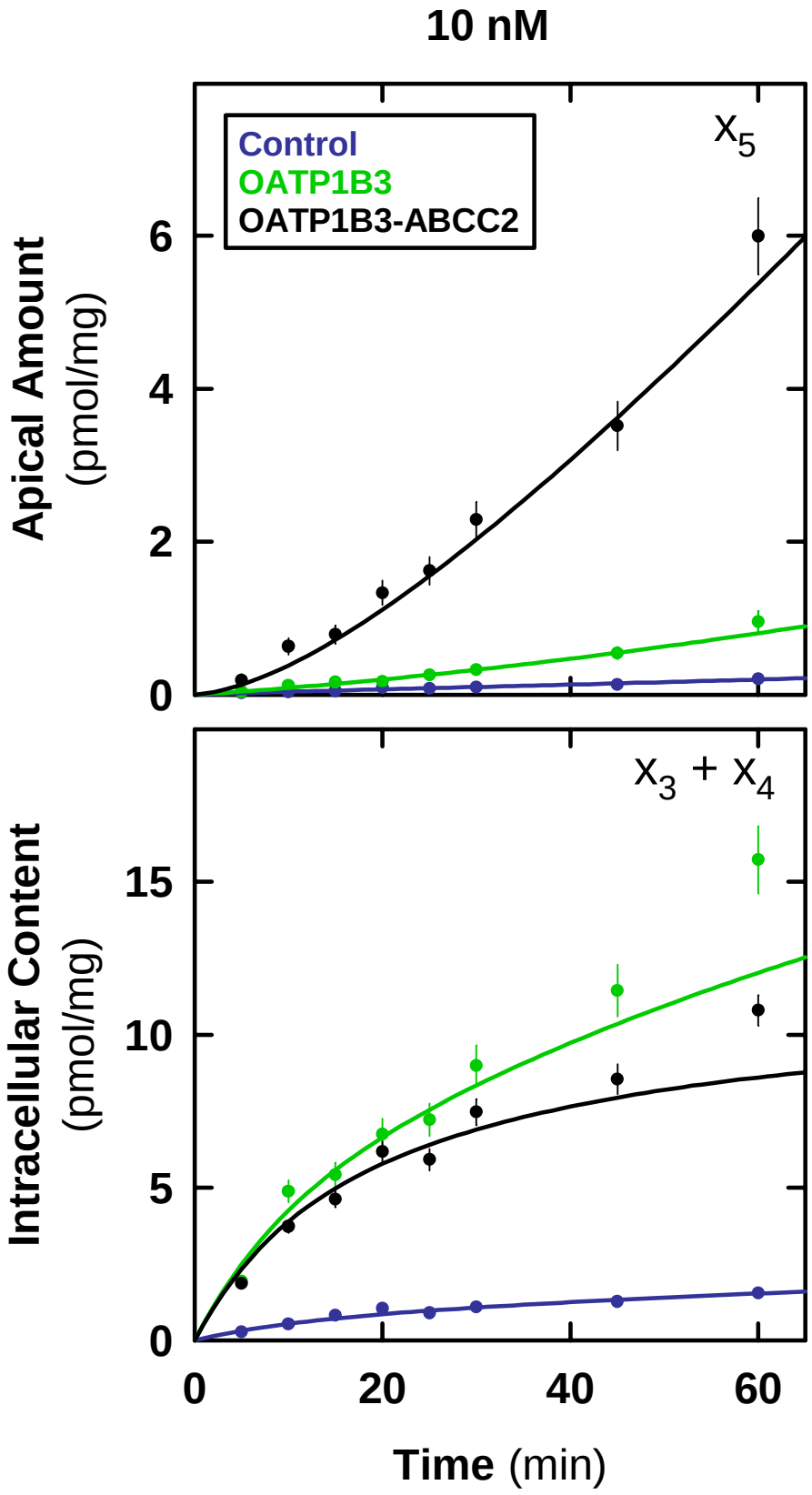

DMD Fast Forward. Published on June 4, 2007 as DOI: 10.1124/dmd.107.015636
This article has not been copyedited and formatted. The final version may differ from this version.

Fig. 5

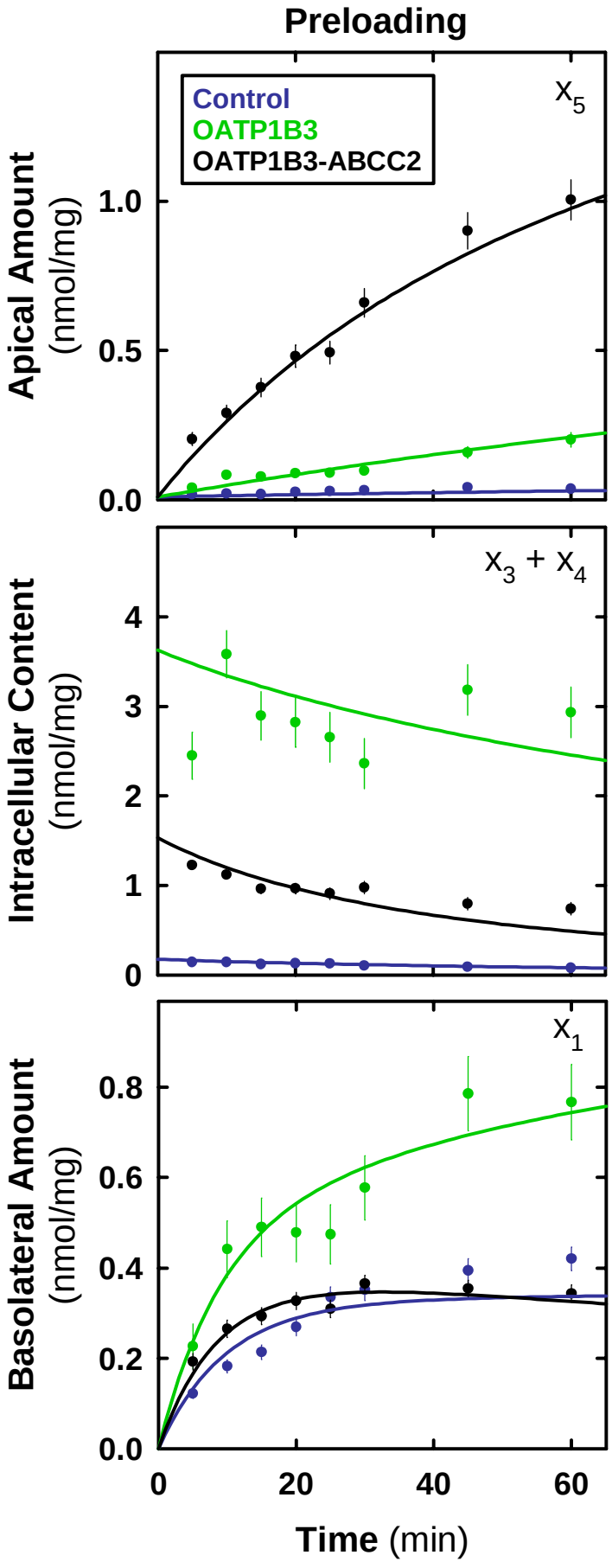

DMD Fast Forward. Published on June 4, 2007 as DOI: 10.1124/dmd.107.015636
This article has not been copyedited and formatted. The final version may differ from this version.

Fig. 6

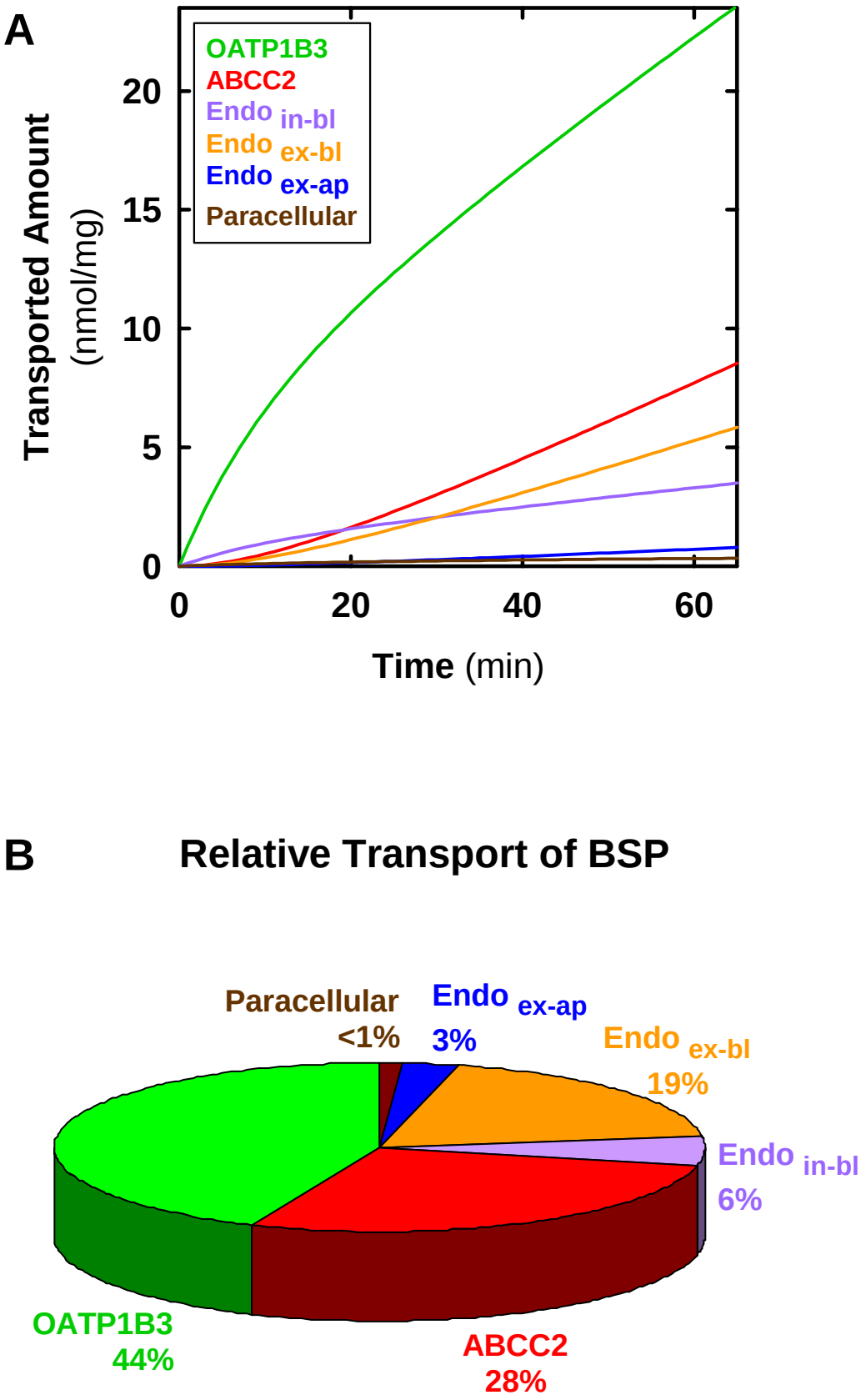

DMD Fast Forward. Published on June 4, 2007 as DOI: 10.1124/dmd.107.015636
This article has not been copyedited and formatted. The final version may differ from this version.

Fig. 7